Hozjan, T., Turk, G. Srpčič, S. 2007. Fire analysis of steel frames with the use of artificial neural networks. Journal of Constructional Steel Research 63, 10: 1396–1403. DOI: 10.1016/j.jcsr.2007.01.013

Fire Analysis of Steel Frames with the use of Artificial Neural Networks

T. Hozjan[a,b], G. Turk[a], S. Srpčič[a,] *

[a] *University of Ljubljana, Faculty of Civil and Geodetic Engineering, Jamova 2, SI-1115 Ljubljana, Slovenia*

[b] *Trimo d.d., Prijateljeva cesta 12, 8210 Trebnje, Slovenia*

Abstract

The paper presents an alternative approach to modelling the mechanical behaviour of material when exposed to high temperatures as expected in fires. Based on series of stress-strain curves obtained experimentally for various temperature levels the artificial neural network (ANN) is employed in material modelling of steel. Geometrically and materially non-linear analysis of plane frame structures subjected to fire is performed by FEM. The numerical results of a simply supported beam are compared with measurements showing good agreement although the temperature-displacement curves exhibit rather irregular shapes. It can be concluded that the ANN is an efficient tool for modelling the material properties in fire engineering design studies.

Key words: steel beam, fire analysis, artificial neural networks, material modelling

* Corresponding author. Phone.: +386 1 47 68 619; Fax: +386 1 47 68 629
E-mail address: ssrpcic@fgg.uni-lj.si (S. Srpčič[a,]).

1 Introduction

In the majority of technical codes the term fire resistance corresponds to the experimentally verified endurance of individual structural elements or minor structural assemblages with regard to standardised heating mode in a test furnace. The standard experimental procedures for determination of fire resistance and the testing based empirical formulae usually describe the local behaviour of the structural element rather reliably. However, even accurate results of experiments in a test furnace do not provide an adequate explanation of the mechanism of global behaviour of composed structure as a whole in a real fire.

Generally, the fire resistance of whole statically indeterminate framed structures is considerably greater than that of the individual structural components. Considering the cost of full-scale tests the development of the research methods is increasingly oriented towards methods of numerical modelling of complex thermo-dynamical and thermo-mechanical problems connected with fire engineering problems. Only efficient numerical algorithms and corresponding software make it possible to perform a large number of parametric studies on the influence of various parameters on the mechanical response of the structure caught by fire. However, the significance of the experimental work does not diminish within this development. On the contrary, experimental data about thermo-dynamical and thermo-mechanical properties of materials and structural elements are the necessary basis for any computational analysis and their required reliability increases with the efficiency and accuracy of available computing tools.

Recent numerical procedures for mechanical analysis of load bearing structures when exposed to fire are mostly based on finite elements with various levels of non-linearity and sophistication combined with non-linear material models calibrated with regard to experimental results. However, there are several uncertainties related to the influence of temperature gradients and the development of plastic and viscous strains at temperatures above 400°C.

Experimental investigations of viscous effects of mild steel published as early as 1967 to 1988 by Stanzak, Harmathy, Williams-Leir, Anderberg [1,2,3,4] and others show that in the temperature range above 400°C and in the regular stress range the creep strains appear in the elements of the structure. At about $500 - 550$°C the creep strain rates become pronounced and the creep strains often prevail over elastic and plastic strains. Considering the standard experimental procedures at uniaxial tests at high temperature and ordinary stress state, it is very difficult to distinguish between the time dependent creep strains and the time-independent plastic strains.

In order to avoid the ambiguities described above we have recently witnessed various attempts to capture the inelastic part of the material model just by a proper set of time-independent stress-strain curves at various temperatures involving both plastic and viscous effects. Characteristic samples are the material models proposed by Eurocode 3 [5] and BS5950 [6] wherein the parameters of temperature dependent bilinear diagrams with elliptic intermediate part are given. As has been stated by Huang and Tan [7] the heating rate and the duration of elevated temperatures have considerable influence on the development of strains and stresses over the structure. Consequently the time-independent material models are only suitable in the cases when the temperature of the steel does not exceed 450°C. In real fire such temperature regime can only

be expected (i) at heat-protected structures when the exposure to the highest temperatures does not last for too long or (ii) at very low stock of combustion material not allowing the fire to develop to full extent. In others, more realistic cases, the experimental data obtained at certain temperature-time curve like ISO 834 or constant heating rate are only of limited applicability.

A relatively abundant set of results of uniaxial tests on structural steel at constant specimen heating rate of 10°C/min has been provided by Kirby and Preston [8] for two steel qualities (Grades 43A and 50B). The data are given in tabular form as two series of stress-strain pairs at various temperature levels for the strains up to 2% in the temperature interval from 20°C to 900°C. In the temperature interval from 250°C to 600°C the irregular wavy shapes of the stress-strain curves do not allow to be approximated by bilinear model with either elliptic or parabolic intermediate part.

Based on the same data Burgess et al. [9] successfully and efficiently modelled the slightly wavy stress-strain curves by Ramberg-Osgood equation.

In the present work the idea of employing the artificial neural network (ANN) was introduced in order to describe the stress-strain-temperature relations. Some difficulties appearing within the course of modelling the properties of steel at elevated temperatures by the ANN have been solved by combining the ANN results with linear regression in the linear elastic range and with linear extrapolation in the hardening range.

2 Artificial neural network

The basic idea and the motivation for the early developments of artificial neural networks (ANN) was the study of the structure and processes in human brain, which is in several aspects similar to the ANN. They both have units called neurons which are interconnected. Similarly to a human brain, the ANN has to be taught or trained. There are two types of learning procedures: supervised, in which questions and answers are known and the ANN has to learn the correct answers; and unsupervised learning, where the answers are not known.

The ANN is a network of simple units (neurons) which operate locally. The units are connected by connections which may reduce or amplify the signal from one unit to another. Each unit receives signals from other units, processes these signals and transmits the signals to other units.

There are several types of ANN geometry. A review of different ANN's is given in several papers, books and Internet sites (e.g. [10,11]). The multi-layer feed-forward network is usually chosen, if functional approximation is sought. Since it is our aim to approximate the strain-stress relation, the multi-layer feed-forward network trained by the supervised learning was chosen.

There are many applications of ANN in structural engineering. Recently, there have been reports on the use of ANN in the modelling of fatigue crack growth [12,13], the modelling of the mechanical properties of steels [14], the modelling of the load carrying capacity of steel struts [15], the modelling of confined reinforced columns [16,17], the modelling of steel columns strength under fire [18] and other interesting applications [19,20].

2.1 Multi-layer feed-forward network

The geometry of a multi-layer feed-forward neural network is shown in Figure 1. Input units are connected to the first layer of hidden units which are further connected to the units of the second hidden layer. The units of the last hidden layer are connected to the output units. The multi-layer feed-forward networks are usually employed for the approximation of the unknown functional relation.

The input units represent the input data, and the output units represent the output data. The hidden layers and all the connections between the units may be considered as a black box which performs the necessary transformations of the input data so that the target output data are obtained.

Each unit is represented by its value y_i^k. Each connection between the units is represented by its weight w_{ij}^k. The index i corresponds to the unit number of the k^{th} layer, while index j corresponds to the unit number of the $(k-1)^{\text{th}}$ layer. The input layer is denoted by 0 and the output layer is denoted by n_l. The signals travel in only one direction, i.e. from the input layer towards the output layer. The value of a unit y_j^{k-1} is multiplied by the corresponding weight w_{ij}^k and added to the value of the signal in the unit of the next layer. In addition, the value of bias neuron or threshold ϑ_i^k is added to the equation

$$y_i^k = \mathrm{f}\left(\sum_{j=1}^{n_{k-1}} w_{ij}^k \, y_j^{k-1} + \vartheta_i^k\right). \tag{1}$$

This equation is illustrated in Figure 1 in which bias neurons are not shown since each bias neuron is connected to only one regular neuron and is not connected to any other neuron. The activation function f(.) enables the modelling of an arbitrary non-linear relation between input and output variables.

Different functions could be used as an activation function, the usual choices being a sigmoid function

$$\mathrm{f}(y) = \frac{1}{1+e^{-y}},$$

$\tanh y$, or Gaussian. The behaviour of the neural network depends on the values of the weights w_{ij}^k and thresholds ϑ_i^k which have to be determined by the learning (training) procedure.

The set of known input and output values is termed an input-output pair. All input-output pairs are often divided into two sets. The first one is termed as learning or training set which is used to determine the connection weights w_{ij}^k and thresholds ϑ_i^k. When the learning procedure ends, meaning that the neural network performs adequately for all input-output pairs in the learning set, the neural network is assessed on the testing set of data.

In some cases the training procedure becomes ill-conditioned if the input and/or output data are not normalised (see e.g. [11]). Therefore, for numerical reasons the values of input and output units have to be normalized. The normalization of the values of output units depends on the range of activation function. Usually, the linear transformation works well, although sometimes a non-linear transformation may help if the data are clustered.

The supervised learning is in fact a general optimization problem in which the minimum of error E_p is sought

$$E_p = \frac{1}{2}\sum_{i=1}^{n_o}\left(t_{pi} - y_{pi}^{n_l}\right)^2, \tag{2}$$

where t_{pi} are the target output values, $y_{pi}^{n_l}$ are the values of neurons in the output layer n_l, i.e. the output values evaluated by the ANN, n_o is the number of neurons in the output layer, i.e. the number of output variables.

This problem is numerically very demanding since a large number of local minima usually exist. There are two essentially different approaches: error back-propagation algorithms which are basically a gradient method and genetic algorithms which are in fact a stochastic search.

The parameters, i.e. the number of hidden layers and the number of hidden neurons of the optimal neural network, are problem dependent. If the number of units is very large, the learning procedure may be very slow, since each forward calculation takes a substantial computational effort. Although larger networks are usually able to learn the sought relationship, this may sometimes be a drawback. A large network may easily reproduce the training set of input-output pairs but fails to generalize, yielding a poor testing performance. Networks with insufficient units may have problems to learn properly during the learning procedure.

3 Material model

The material model, later used in the mechanical analysis, was constructed by the ANN on the basis of experimental data [8]. The neural network was thought to estimate stress σ, while strain ε and temperature T were used as input data. The calculation was carried out for steel strength $f_{\mathrm{y}} = 35.5\,\mathrm{kN/cm^2}$. All 527 input-output pairs were divided into two sets: learning and testing set. Different sizes of learning and testing sets were tried, however the results did not differ considerable. Finally, 435 randomly selected pairs were used for learning and the remaining 92 were used as testing pairs.

The allowed relative error was set to 0.05, which is a relatively low value

in an ANN training procedure. Many calculations with different geometry of neural network were carried out. On the basis of results the final solution was calculated with the geometry 2-50-50-1, i.e. there were two hidden layers, each of them including 50 neurons. The efficiency of learning procedure is shown in Figure 2, where actual and calculated values belonging to testing set are compared. In this case the coefficient of correlation was very high: $r^2 = 0.9993$.

The results of the ANN are shown in Figure 3, which represents the stress-strain relationship at different temperature levels T. The experimental data of stress are shown with rombic marks, while calculated values are presented with a continuous line.

The accordance between the calculated values obtained by the ANN and the experimental ones is very good along the entire $\sigma - \varepsilon$ curve for all temperature levels.

However, some difficulties appear within the course of modelling the properties of steel at elevated temperatures by the ANN. Firstly, the yield points of particular stress-strain curves are not explicitly defined by the curve shape itself. The problem was solved by plotting the first derivatives of the experimentally obtained stress-strain relations where the yield limits are much better pronounced. Secondly, due to the regressions used in the ANN the obtained approximations for the stress-strain relations below the yield limit exhibit certain deviations from a linear shape. Assuming ideal linear behaviour of steel the linear regression based on actual experimental data has been used for this range. Lastly, since the experimental data are given for the values of strains of up to 2%, the ANN model is inadequate for the range of strains higher than 2% and a constant hardening parameter is introduced in this strain range.

According to that, the presented material model is divided into three parts (Figure 4). The first part is linear elastic $\varepsilon_M < \varepsilon_Y$ and the stress σ is determined by linear elastic law

$$\sigma(\varepsilon_{\mathrm{M}}, T) = E_{\mathrm{T}}\varepsilon_{\mathrm{M}} = k_{\mathrm{E,T}}E_{20}\varepsilon_{\mathrm{M}}, \tag{3}$$

where $k_{\mathrm{E,T}}$ stands for reduction factor of the elastic modulus, describing its variation in dependency of the temperature T refering to the elastic modulus E_{20} at the room-temperature $T = 20°\mathrm{C}$.

The second part stands for the plastic range where the mechanical strain exceeds the yield strain $\varepsilon_{\mathrm{M}} > \varepsilon_{\mathrm{Y}}$. In this range, the stress is calculated by the ANN, in accordance with the actual values of the mechanical strain ε_{M} and temperature T

$$\sigma(\varepsilon_{\mathrm{M}}, T) = f_{\mathrm{ANN}}(\varepsilon_{\mathrm{M}}, T). \tag{4}$$

In the range where the mechanical strain exceeds the value of $\varepsilon_{\mathrm{M}} > 1.85\%$, a uniform strain-hardening parameter K is considered. The value of K is determined by the slope of the stress-strain curve at the strain $\varepsilon_{\mathrm{M}} = 1.85\%$ and at the corresponding temperature T ($K = K(\varepsilon_{\mathrm{M}} = 1.85\%, T)$).

The yield strain ε_{y} and the reduction factors $k_{\mathrm{y,T}}$ and $k_{\mathrm{E,T}}$ are determined on the basis of experimental data [8]. The reduction factors compared with those prescribed by Eurocode 3 [5] are shown in Figure 5.

We should note that experimental data [8] are determined at the heating rate 10°C/min and therefore the applicability of this material model is limited. The authors mention that the results for these heating rates are quite similar to the results obtained by other researchers, whose measurements were performed at different heating rates, namely 2.5°C/min, 5°C/min and 20°C/min. With this

statement the application of the presented model at different heating rates is acceptable, when provided that the heating rate does not differ from 10°C/min excessively.

4 Beam theory

The analysis of beam elements is based on the presumption that particular longitudinal filaments of the element are exposed to uniaxial stress state. In this case the results of uniaxial tests are of direct relevance for the formulation of constitutive relations. This means that we have to deal with physical values of stresses and strains which refer to the initial, non-deformed state of the element. It can also be presumed that the temperature of any point of the element is a known function of time $T = T(t)$. In order to consider the geometrically and materially non-linear behaviour of an element, the relation between strain ε, temperature T, time t and longitudinal normal stress σ shall be found in an incremental form. In this paper, in spite of the doubts about its suitability at high temperatures, the additive principle is adopted, where the geometrical strain increment $\Delta\varepsilon$ is a sum of the mechanical part $\Delta\varepsilon_M$, temperature part $\Delta\varepsilon_T$ and viscous part $\Delta\varepsilon_C$

$$\Delta\varepsilon = \Delta\varepsilon_M + \Delta\varepsilon_T + \Delta\varepsilon_C \,. \tag{5}$$

All the increments refer to the time step $[t^{(n)}, t^{(n+1)}]$.

4.1 The strain increment due to temperature change

In this paper the strain increment $\Delta\varepsilon_T$ induced by the temperature change $\Delta T = T^{(n+1)} - T^{(n)}$ is determined according to Eurocode 3: prEN 1993-1-2 [2] where the total temperature strain is given for three characteristic temperature ranges

$$\begin{aligned}
&20°\mathrm{C} \leq \mathrm{T} < 750°\mathrm{C}: \quad \varepsilon_T = 1.2 \cdot 10^{-5}\, T + 0.4 \cdot 10^{-8}\, T^2 + -2.416 \cdot 10^{-4},\\
&750°\mathrm{C} \leq \mathrm{T} \leq 860°\mathrm{C}: \quad \varepsilon_T = 1.1 \cdot 10^{-2},\\
&860°\mathrm{C} < \mathrm{T} \leq 1200°\mathrm{C}: \quad \varepsilon_T = 2 \cdot 10^{-5}\, T - 6.2 \cdot 10^{-3}.
\end{aligned}$$

After calculating the total temperature strains $\varepsilon_T^{(n)}$ at the beginning and $\varepsilon_T^{(n+1)}$ at the end of the time step considered, the temperature strain increment is obtained simply by the difference

$$\Delta\varepsilon_T = \varepsilon_T^{(n+1)} - \epsilon_T^{(n)}. \tag{6}$$

4.2 The strain increment due to the creep of the steel

Harmathy's [1] model based on the general Dorn's theory of viscous creep has been proved to be a rather good tool for simulation of the time dependent behaviour of metals at elevated temperatures. A modified form of Harmathy's model was published by Williams-Leir [3] relating the creep strain ε_C to the real time t

$$\frac{d\varepsilon_C}{dt} = \mathrm{sign}(\sigma)\, b_1 \coth^2(b_2|\varepsilon_C|). \tag{7}$$

On the basis of numerous experiments Williams-Leir [3] provided analytical expressions for the creep parameters b_1 and b_2 for various kinds of structural steel in terms of the absolute temperature T [K] and actual stress level

$\sigma\,[\mathrm{lbf/in^2}]$. Within the incremental approach, the creep equation (7) can be employed in every short time interval $\Delta t = t^{(n+1)} - t^{(n)}$, although it has been derived under the assumption of constant temperature and stress. By these means, the creep strain increment is given by the following relation

$$\Delta\varepsilon_C = \mathrm{sign}\,(\sigma)\, b_1 \coth^2(b_2|\varepsilon_C|)\, \Delta t. \tag{8}$$

However, in the present work the ANN material model based on experimental data [8] is assumed to contain elastic, plastic and creep strains. Therefore, the increment of the creep strain does no longer explicitly take place in the additive principle (5).

4.3 The mechanical strain increment

The mechanical strain increment $\Delta\varepsilon_M$, which originally does not explicitly depend upon time and temperature and is related to the longitudinal normal stress by the parameters of a uniaxial test, consists of an elastic part $\Delta\varepsilon_E$ and a plastic part $\Delta\varepsilon_P$

$$\Delta\varepsilon_M = \Delta\varepsilon_E + \Delta\varepsilon_P = \Delta\varepsilon - \Delta\varepsilon_T \tag{9}$$

An essential step towards the determination of the stress-strain state of an arbitrary point of the cross-section at the end of the time step $[t^{(n)}, t^{(n+1)}]$ is the introduction of an auxiliary state [21] which is not necessary an actual stress state. Assuming that all relevant quantities at the initial time $t^{(n)}$ are

known we first consider the trial purely elastic step defined by the formulas

$$\begin{aligned}
\sigma^{(n+1)^{trial}} &= \sigma^{(n)} + \Delta E\, \varepsilon_E^{(n)} + E^{(n+1)} \Delta\varepsilon_M, \\
\xi^{(n+1)^{trial}} &= \sigma^{(n+1)^{trial}} - q^{(n)}, \\
\varepsilon_P^{(n+1)^{trial}} &= \varepsilon_P^{(n)}, \\
\gamma^{(n+1)^{trial}} &= \gamma^{(n)}, \\
q^{(n+1)^{trial}} &= q^{(n)}, \\
f^{(n+1)^{trial}} &= |\xi^{(n+1)^{trial}}| - \sigma_Y.
\end{aligned} \tag{10}$$

In the equations listed above ε_E and ε_P are the total elastic and plastic strains respectively, while $\Delta E = E^{(n+1)} - E^{(n)}$ denotes the change of the modulus of elasticity corresponding to the time interval $[t^{(n)}, t^{(n+1)}]$. In order to simulate the Bauschinger effect by means of kinematic hardening model, the relative stress ξ is introduced in dependency of the back-stress q which describes the centre of the actual yield surface. $\gamma > 0$ is the accumulated plastic strain and σ_Y is the actual yield limit. The auxiliary yield function f^{trial} defines the status of the point at the end of the time step. If $f^{(n+1)^{trial}} \leq 0$ there is an elastic step and the trial state coincides with the actual stress-strain state at the time $t^{(n+1)}$

$$\begin{aligned}
\sigma^{(n+1)} &= \sigma^{(n+1)^{trial}}, \\
\varepsilon_P^{(n+1)} &= \varepsilon_P^{(n+1)^{trial}}, \\
\gamma^{(n+1)} &= \gamma^{(n+1)^{trial}}, \\
q^{(n+1)} &= q^{(n+1)^{trial}}.
\end{aligned} \tag{11}$$

The alternative case, if $f^{(n+1)^{trial}} > 0$, denotes a plastic step characterised by the absolute increment $\Delta\gamma$ of the plastic strain

$$\Delta\gamma = \frac{|\sigma^{(n+1)^{trial}}| - \mathrm{sign}(\sigma^{(n+1)^{trial}})\, \sigma^{(n+1)}}{E^{(n+1)}} > 0. \tag{12}$$

In this case the stress-strain state at the time $t^{(n+1)}$ is defined by the following formulas

$$\begin{aligned}
\sigma^{(n+1)} &= \sigma^{(n+1)^{trial}} - \Delta\gamma\, E^{(n+1)}\, \mathrm{sign}(\xi^{(n+1)^{trial}}),\\
\varepsilon_P^{(n+1)} &= \varepsilon_P^n + \Delta\gamma\, \mathrm{sign}(\xi^{(n+1)^{trial}}),\\
q^{(n+1)} &= q^{(n)} + \Delta\gamma\, H\, \mathrm{sign}(\xi^{(n+1)^{trial}}),\\
\gamma^{(n+1)} &= \gamma^{(n)} + \Delta\gamma.
\end{aligned} \tag{13}$$

Here H is the elastoplastic tangent modulus. When using the bilinear material model, the elastoplastic tangent modulus can be expressed by the plastic modulus K with the relation

$$H(T) = \frac{E(T)\, K(T)}{E(T) + K(T)} \tag{14}$$

4.4 Program POZAR

The constitutive relations described in the preceding section have been incorporated into the computer program POZAR. The program uses a novel finite element formulation to determine the mechanical response of the planar frame [22,23,24] subjected to time variable mechanical and temperature load. The formulation is based on the modified Hu-Washizu [25] functional for the kinematically exact planar beam theory of Reissner [26]. The only unknown functions in the functional, the extensional strain, ε, and the pseudo-curvature, κ, are approximated by the Lagrangian interpolation scheme. The remaining unknown functions, i.e. displacements, the rotation and the internal forces and moments, appear in the functional only through their boundary values. The finite element formulation yields a system of discrete generalized equilibrium equations of the structure which is solved by the Newton incremental iterative method.

5 Numerical example

A simply supported beam was analysed with the aim to verify the material model and numerical algorithms used. The numerical results were compared with the experimental ones published by Rubert and Schaumann [27] who carried out several elevate temperature tests on simply supported beams under simultaneous mechanical and thermal loading. The beams, having an IPE 80 cross-section (DIN 1025-1) and the length of 1.14 m, were subjected to a constant midspan concentrated load and then heated uniformly along their entire length (Figure 6).

In this paper, eight finite elements were used for modelling the beam. For the elastic modulus and yield strength at the room temperature $T = 20°\mathrm{C}$, the value from experiment [8] was used: $E_{20} = 19200\,\mathrm{kN/cm^2}$ and $f_{\mathrm{y},20} = 35.5\,\mathrm{kN/cm^2}$. When testing the beam, four different load utilisation factors $\eta = 0.20,\ 0.50,\ 0.70,\ 0.85$ were considered, representing the ratios of the applied loads to the ultimate load carrying capacity at room temperature. Since the values of the yield strength $f_{\mathrm{y},20}$ at different load ratios η were different, suitable loads were calculated according to different η (Table 1) in order to compare the results of the midspan displacement w.

In addition to the material model described above, a material model according to the Eurocode 3 [5] standard and a bilinear material model [28] were also considered. When the bilinear material model was discussed, the creep of steel (Austen 50) [3], was taken into consideration.

The midspan displacements w obtained numerically using three material models are shown in Figure 7. In the case of the ANN material model, the results

are in very good agreement with the experiment at all load ratios η. On the other hand, this statement does not apply for the bilinear model. Although the accordance at lower load ratios is good, at higher load ratios the difference increases thus indicating that the creep strains are already included in the time independent results of uniaxial tests. The material model according to the Eurocode 3 standards yields rather good accuracy at lower load ratios, while at higher load ratios the difference is noticeable, especially in the range where the displacement w exhibits irregular behaviour.

The development of plastic strain ε_{P} at the bottom of the mid-section with respect to raising temperature T is shown in Figure 8. The differences between the bilinear model and other two models become evident at relatively low temperatures due to the fact that it is virtually impossible to reliably simulate steel behaviour at elevated temperatures by bilinear model. The initial development of plastic strains in the cases of the ANN and Eurocode models is similar. The differences at high temperature stem from the fact that in the case of Eurocode model the material hardening is not considered.

Figure 9 shows the time dependent development of strains and stresses at the bottom and at the top of the middle cross-section for the case of the ANN material model.

Furthermore, in Figure 10 the distribution of stress and strains over the middle cross-section is shown for five characteristic time steps also showing the percentage of the already plastified part of the cross-section. The latter data are more important in real fire scenarios, where the residual stresses and strains have to be determined in order to estimate the eventual further usage of the beam.

6 Conclusions

The paper presents a non-linear analysis of steel frames subjected to fire. The main emphasis is on the use of artificial neural network (ANN) in the formulation of the material model of structural steel at elevated temperature levels on the basis of experimental data. This way, very good agreement of numerically determined displacements of the test beam with experimental results was achieved even at higher load ratios. The employment of ANN proved to be an improvement with respect to commonly used material models since the latter show considerably larger errors for higher load ratio when compared to experimental results (see Fig. 7).

So far, the conclusion is limited with regard to the steel yield strength $f_{\mathrm{y}} = 35.5$ kN/cm^2 and to the heating rate 10°C/min. Nevertheless, the results allow the assumption that the procedure can be succesfully applied also to other kinds of steel and different heating rates. It shall also be noted that the time dependent creep strain is ment to be included in the plastic, time independent range of the presented material model. Numerous more demanding experimental tests should be carried out in order to obtain more information on the inelastic range of steel behaviour at elevated temperatures with special atention to treating the relations between plastic and time dependent creep strains.

7 Acknowledgement

The work of T. Hozjan was financially supported by the Ministry of Education, Science and Sport of the Republic of Slovenia and by the Ministry of the Economy of the Republic of Slovenia under contract 3311-04-831816. The support is gratefully acknowledged.

References

[1] Harmathy TZ. A Comprehensive Creep Model. Journal of Basic Engineering 1967;89(D-3):496-502.

[2] Harmathy TZ, Stanzak WW. Elevated-Temperature Tensile and Creep Properties of Some Structural and Prestressed Steels. American Society for Testing and Materials, Special Technical Publication 464 on Fire Test Performance 1970:186-208.

[3] Williams-Leir G. Creep of structural steel in fire: Analytical expressions. Fire and Materials 1983;7(2):73-78.

[4] Anderberg Y. Modelling Steel Behaviour. Fire Safety Journal 1988;13(1):17-26.

[5] Eurocode 3: Design of steel structures. Part 1.2: General rules-Structural fire design. Brussels: European Committee for Standardisation; 2001.

[6] British Standard Institute, BS5950-8:Structural Use of Steelwork in Building - Part 8: Code of Practice for Fire Resistance Design. London: British Standards Institution; 2003.

[7] Huang ZF , Tan KH. Effects of External Bending Moments and Heating Schemes on the Responses of Thermally-restrained Steel Columns, Engineering Structures 2004;26(6):769-780.

[8] Kirby BR, Preston RR. High temperature properties of hot-rolled, structural steels for use in fire engineering design studies. Fire Safety Journal 1988;13:27-37.

[9] Burgess, IW, Olawale AO, Plank RJ. Failure of steel column in fire. Fire Safety Journal 1992;18:183-201.

[10] Lippmann RP. An Introduction to Computing with Neural Nets. IEEE Magazine on Acoustics, Signal and Speech Processing 1987;4(2):4-22.

[11] Sarle WS. Neural Network FAQ. Periodic posting to the Usnet newsgroup comp.ai.neural-nets, URL: ftp://ftp.sas.com/pub/neural/FAQ.html, 2002.

[12] Seed GM, Murphy GS. The applicability of neural networks in modelling the growth of short fatigue cracks. Fatigue & Fracture of Engineering Materials & Structures 1998;21:183-190.

[13] Haque ME, Sudhakar KV. ANN based prediction model for fatigue crack growth in DP steel. Fatigue & Fracture of Engineering Materials & Structures 2001;23:63-68.

[14] Sterjovski Z, Nolan D, Carpenter KR, Dunne DP, Norrish J. Artificial neural networks for modelling the mechanical properties of steels in various applications. Journal of Materials Processing Technology 2005;170:536-544.

[15] Sakla SSS. Neural network modeling of the load-carrying capacity of eccentrically-loaded single-angle struts. Journal of Constructional Steel Research 2004;60:965-987.

[16] Oreta A, Kawashima K. Neural Network Modeling of Confined Compressive Strength and Strain of Circular Concrete Columns. Journal of Structural Engineering 2003;129(4):554-561.

[17] Tang CW; Chen HJ, Yen T. Modeling Confinement Efficiency of Reinforced

Concrete Columns with Rectilinear Transverse Steel Using Artificial Neural Networks. Journal of Structural Engineering 2003;129(6):775-783.

[18] Zhao Z. Steel columns under fire - a neural network based strength model. Advances in engineering software 2004;37(2):97-105.

[19] Mikami I, Tanaka S, Hiwatashi T. Neural Network System for Reasoning Residual Axial Forces of High-Strength Bolts in Steel Bridges. Computer-Aided Civil and Infrastructure Engineering 1998;13:237-246.

[20] Papadrakakis M, Lagaros ND, Plevris V. Design optimization of steel structures considering uncertainties. Engineering Structures 2005;27: 1408-1418.

[21] Simo JC, Hughes TJR. Computational inelasticity. New York: Springer Verlag; 1998.

[22] Bratina S, Saje M, Planinc I. On materially and geometrically non-linear analysis of reinforced concrete planar frames. Internal report 1/2003. Ljubljana: University of Ljubljana; 2003.

[23] Bratina S, Planinc I, Saje M, Turk G. Non-linear fire-resistance analysis of reinforced concrete beams. Structural Engineering and Mechanics 2003;16(6):695-712.

[24] Planinc I, Saje M, Čas B. On the local stability condition in the planar beam finite element. Structural Engineering and Mechanics 2001;12(5):507-526.

[25] Washizu K. Variational Methods in Elasticity and Plasticity. Oxford: Pergamon Press; 1975.

[26] Reissner E. On one-dimensional finite-strain beam theory: The plane problem. Journal of Applied Mathematics and Physics (ZAMP) 1972;23:795-804.

[27] Rubert A, Schaumann P., Temperaturabhangige werkstoffeigenschaften von baustahl bei brandbeanspruchung, Stahlbau 1985;3:81-86.

[28] Srpičič S. Račun vpliva požara na jeklene konstrukcije. PhD thesis. Ljubljana: University of Ljubljana; 1991 (in Slovenian).

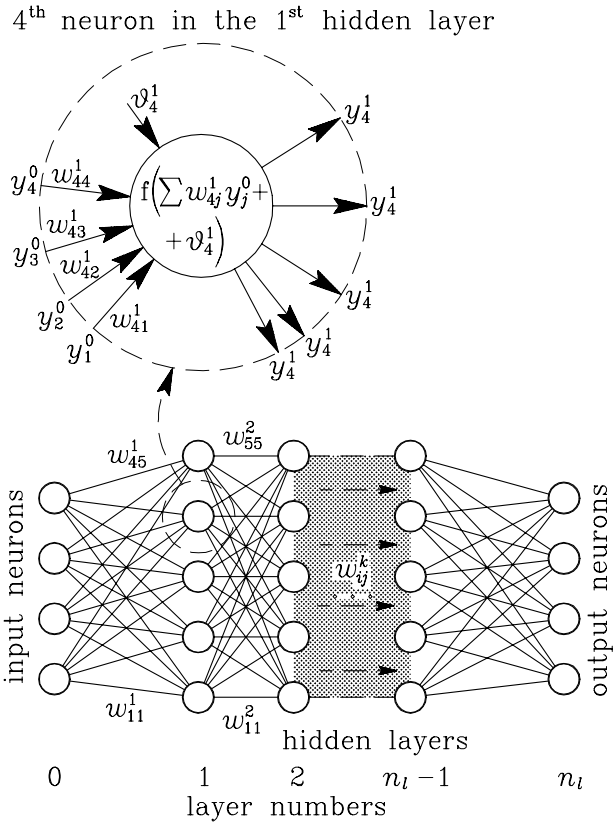
4th neuron in the 1st hidden layer
input neurons
output neurons
hidden layers
0
1
2
n_l-1
n_l
layer numbers

Fig. 1.

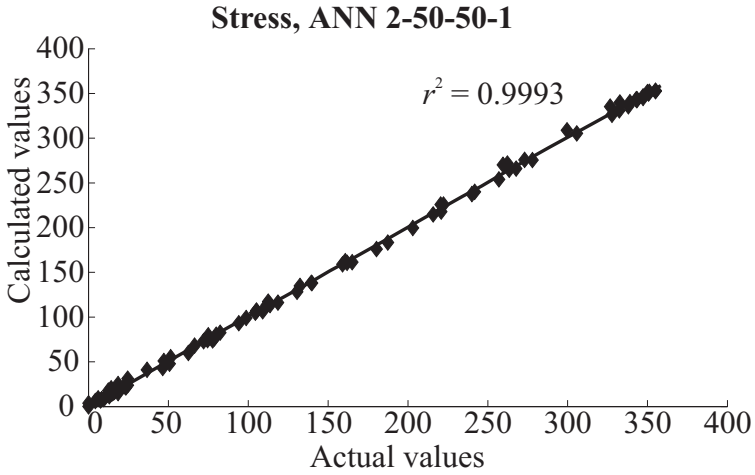
Stress, ANN 2-50-50-1
$r^2 = 0.9993$
Calculated values
Actual values
0
50
100
150
200
250
300
350
400

Fig. 2.

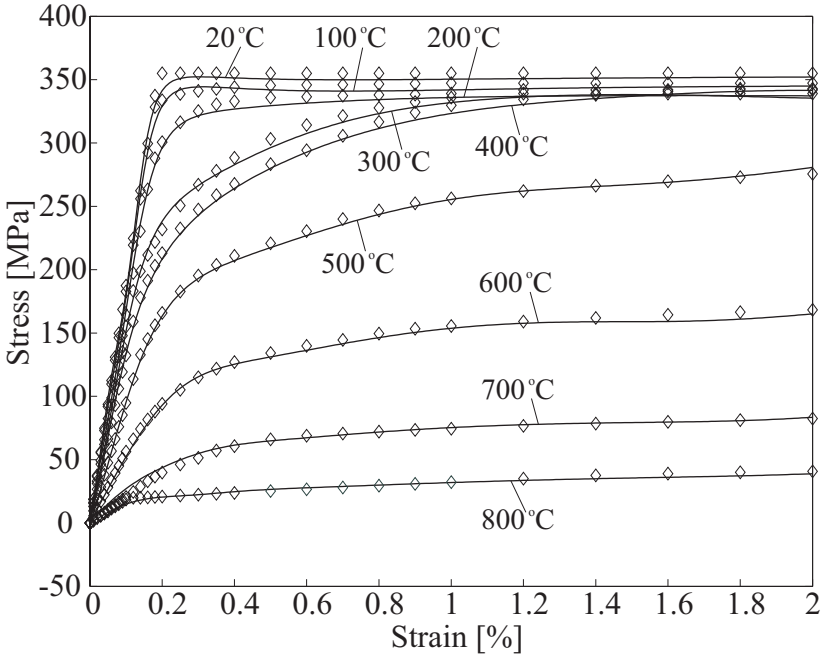
400
350
300
250
200
150
100
50
0
-50
Stress [MPa]
0
0.2
0.4
0.6
0.8
1
1.2
1.4
1.6
1.8
2
Strain [%]
20°C
100°C
200°C
300°C
400°C
500°C
600°C
700°C
800°C

Fig. 3.

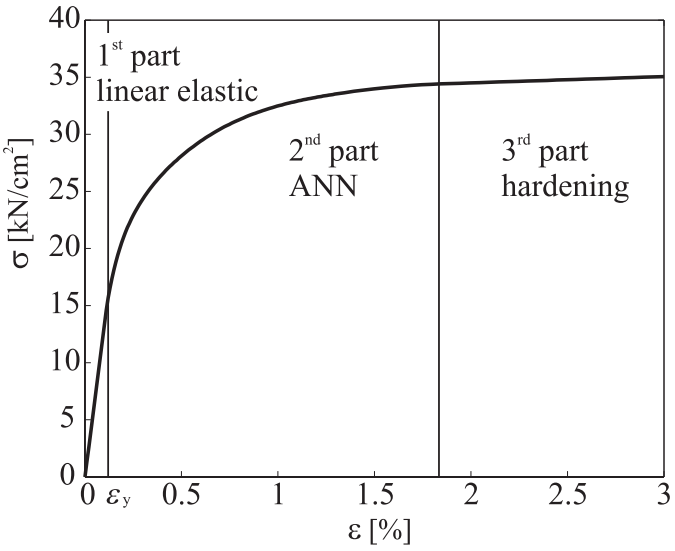
40
35
30
25
20
15
10
5
0
σ [kN/cm²]
1st part
linear elastic
2nd part
ANN
3rd part
hardening
0
εy
0.5
1
1.5
2
2.5
3
ε [%]

Fig. 4.

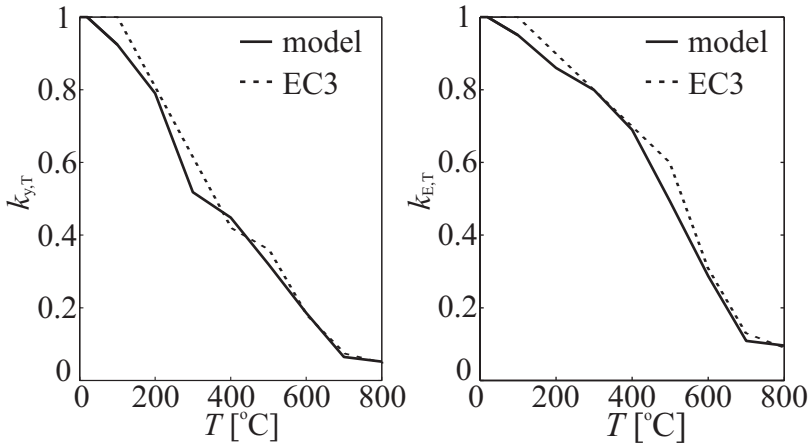
1
0.8
0.6
0.4
0.2
0
$k_{y,T}$
model
EC3
0
200
400
600
800
T [°C]
1
0.8
0.6
0.4
0.2
0
$k_{E,T}$
model
EC3
0
200
400
600
800
T [°C]

Fig. 5.

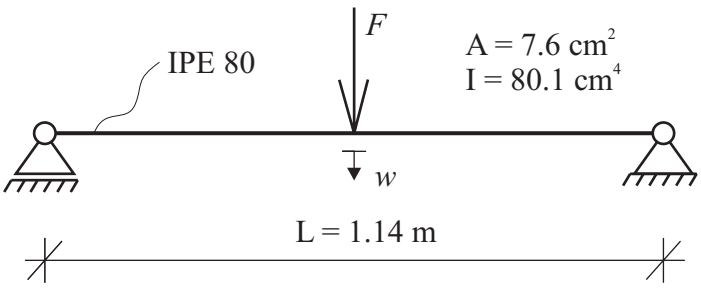

Fig. 6.

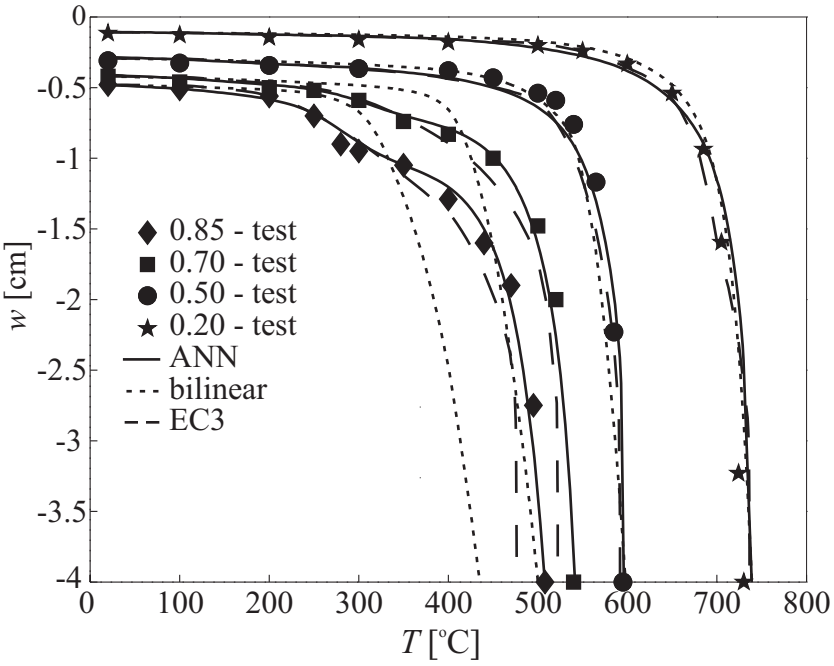
0
-0.5
-1
-1.5
-2
-2.5
-3
-3.5
-4
w [cm]
0.85 - test
0.70 - test
0.50 - test
0.20 - test
ANN
bilinear
EC3
0
100
200
300
400
500
600
700
800
T [°C]

Fig. 7.

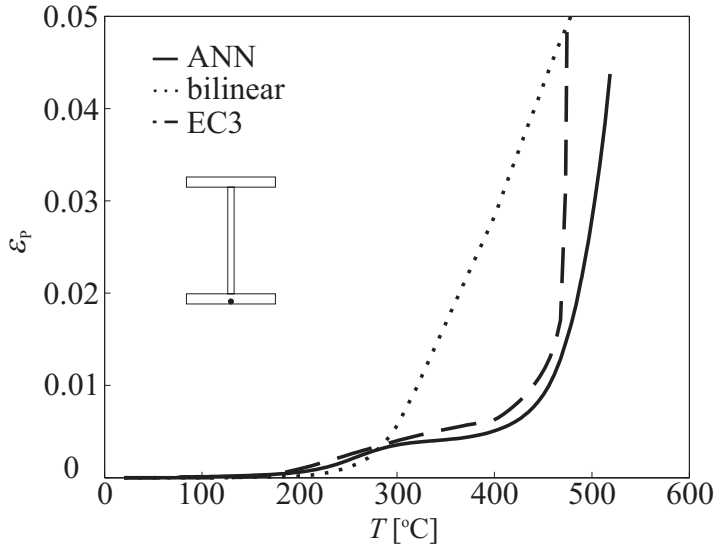
0.05
0.04
0.03
0.02
0.01
0
ε_P
ANN
bilinear
EC3
0
100
200
300
400
500
600
T [°C]

Fig. 8.

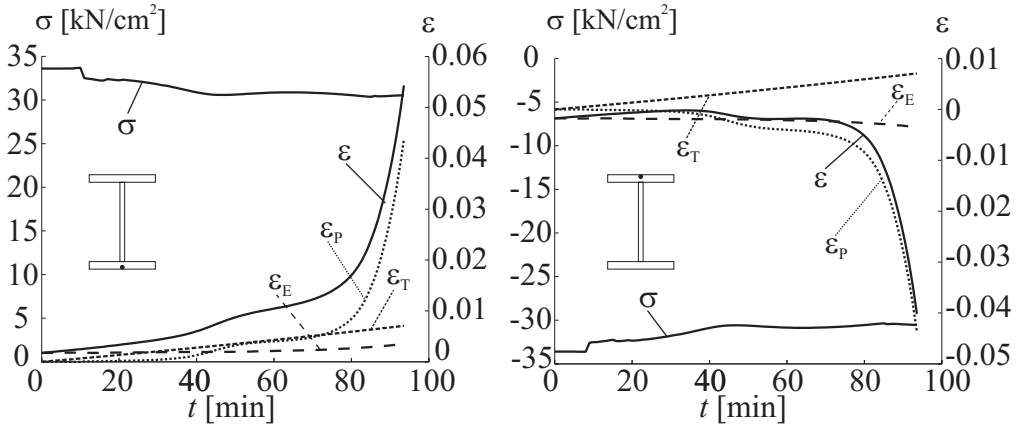
σ [kN/cm²]
ε
σ
ε
ε_P
ε_E
ε_T
t [min]
σ [kN/cm²]
ε
ε_E
ε_T
ε
ε_P
σ
t [min]

Fig. 9.

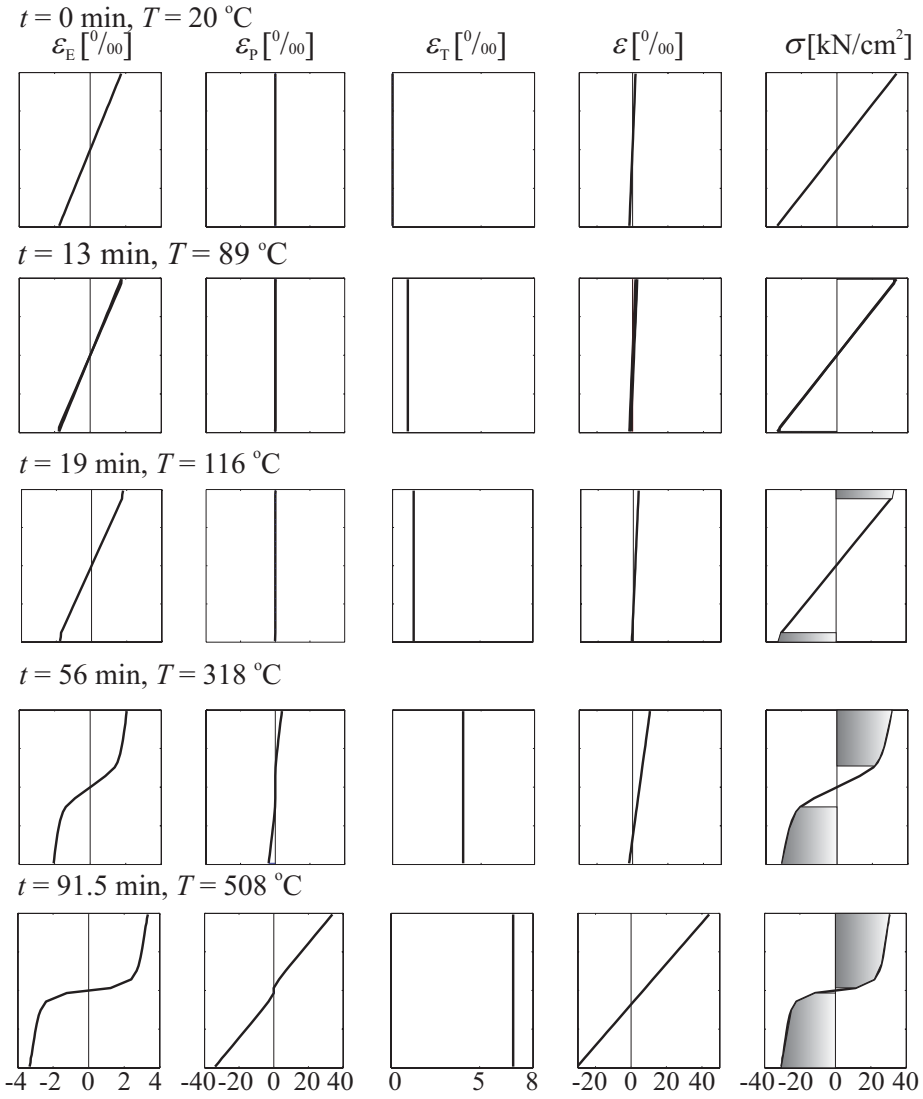
t = 0 min, T = 20 °C
εE [0/00]
εP [0/00]
εT [0/00]
ε [0/00]
σ[kN/cm2]
t = 13 min, T = 89 °C
t = 19 min, T = 116 °C
t = 56 min, T = 318 °C
t = 91.5 min, T = 508 °C
-4 -2 0 2 4
-40 -20 0 20 40
0 5 8
-20 0 20 40
-40 -20 0 20 40

Fig. 10.

Table 1 Calculation values of the force F

load ratio η	f_y experiment [kN/cm^2]	F experiment [kN]	F calculation [kN]
0.85	35.2	24	24.2
0.70	39.9	23	20.5
0.50	39.9	16	14.2
0.20	39.9	6	5.3